

# Tuning the response of bubble-based metamaterials with short transient pulses

Vicky Kyrimi and Kosmas L. Tsakmakidis

*Section of Condensed Matter Physics, Department of Physics, National and Kapodistrian University of Athens, Panepistimioupolis, GR - 157 84, Athens, Greece*

*Correspondence: vicky@phys.uoa.gr*

## Abstract:

Bubble-based metamaterials have been extensively studied both theoretically and experimentally thanks to their simple geometry and their ability to manipulate acoustic waves. The latter is partly dependent on the structural characteristics of the metamaterial and partly dependent on the incident acoustic wave. Initially, the selection of specific structural characteristics is explained by presenting the Fourier transformations of the reflected waves for different arrangements of a bubbly meta-screen subject to Gaussian excitation. Next, our numerical study focuses on the changes induced to the response of a bubbly meta-screen, subject to different excitation pulses. For complex-frequency excitation the bubbles delay to return to their equilibrium position for a couple of moments, hence the energy is stored in the system during those moments. This research provides a new strategy to actively control the response of a bubbly meta-screen and seeks to inspire future studies towards further optimization of the incident pulse based on the functionalities in need.

## Introduction

Underwater energy storage is desirable in many situations. One may want, for instance, to convert the stored energy into electrical energy or to use the existing energy as a means to impart momentum to the surrounding fluid. The longer the time duration the energy carrier interacts with a structure, the most efficient the structure is, in terms of storing energy. Clusters of air bubbles in water ensonified by a time-harmonic acoustic wave are forced to vibrate; they store and then release the energy obtained due to interaction with the energy carrier, the impinging acoustic wave.

Except from storing energy, such structures have attracted extensive attention thanks to their property to shift the frequency of the impinging wave [1-3], to their ability to turn acoustic reflectors into perfect absorbers over a broad frequency range when arranged periodically in two dimensions and placed very close to the reflectors [4], to the observation of i) band-gaps [5], ii) a negative slope in the dispersion relation when arranged in a diamond structure in three dimensions [6], to their surprisingly high transmission when arranged periodically [7] or randomly [8]. The latter is of wide interest and has been associated with the fundamental problem of Anderson localization. Soundproofing, designing under-water sensors and lenses as well as making immersed objects

invisible to sonar are some of the striking applications favored by the above-mentioned properties of clusters of air bubbles in water. Inert gas microbubbles have been used to extract in-plane velocities of blood flow deep into living organs, paving the way for deep super-resolution biomedical imaging [9]. Most of the above-mentioned studies concern plane waves impinging upon clusters of gaseous bubbles and the methodology used to extract reflection and transmission coefficients is based on expressing the incident plane wave as a sum of spherical wave functions, as presented in detail in [10]. Based on the multiple scattering theory approach [11], Skaropoulos et al. have shown that interactions between incident sound waves and bubbles result in higher-order modes only when the bubbles are in close proximity. This means that for larger separations only monopolar scattering takes place. According to [12] a factor larger than 5 between separation distance and bubble radius indicates that the separation is large enough to exclude dipolar responses. For such large separations the interactions persist at the lowest resonance frequency which coincides with that of Minnaert resonance,  $\omega_M = \sqrt{3\gamma p_{eq}/\rho_l R_{eq}^2}$ , (1) where  $p_{eq}$  is the pressure at equilibrium,  $R_{eq}$  is the bubble radius at equilibrium,  $\rho_l$  is the fluid density and  $\gamma$  is the adiabatic constant (given in **Table I**), used for processes where the heat flows across the bubble wall and the thermal exchanges between the gas and the water are ignored. The subscript M comes from Minnaert who published a solution for the acoustic resonance frequency of a single bubble in water and showed that at the resonance frequency the bubble oscillates radially in response to the incident acoustic wave [13]. Recently, high transmission across a bubble layer measured at low frequencies (150-260 kHz) [14], was attributed to the Minnaert-like resonance of two dimensional bubbles, confirming that bubbles are not simple scatterers [15]. Persistent interactions have also been observed in case the incident plane wave is replaced by a short duration pulse. As a result, a wide frequency band around  $\omega_M$  is excited. A bubbly screen stores energy over time much larger than the pulse duration, as shown in [16]. The analysis of the equation of energy conservation in the effective problem indicates that soon after the initial excitation of the bubbly screen the amount of energy stored reaches its maximum value; at exactly that time point, the reflected energy reaches its minimum value. From that time point onwards, the amount of the radiating reflected energy starts increasing whereas the amount of the energy stored in the bubbly screen starts decreasing. Therefore our attention should be focused on how to lengthen the time interval during which the stored energy increases monotonically and allow for long time oscillations. An intuitive approach is to increase inter-bubble distance. For a dense array the pulse decelerates as the sound velocity in a region mainly occupied by gas is much smaller than the sound velocity in water. Hence, the kinetic energy is turned into radiation. For large inter-bubble distance radiative damping is small as there is no abrupt change in the kinetic energy but as a counterpart, the interaction between the incident pulse and the screen is weak.

An alternative approach to induce long oscillation duration and strong interaction between the incident pulse and the bubbly layer for an intermediate inter-bubble distance has been used in the present work. We use a shorter duration pulse compared to the previously reported case and we demonstrate the delay of the oscillating bubble to return to its equilibrium position. Strong interaction between the incident acoustic pulse and the bubbly layer is also shown.

## Background

A periodic arrangement of identical, penetrable spheres of radius  $R_{eq}$  in an unbounded, homogeneous liquid is shown in **Fig. 1**. The separation distance between spheres is  $h$ . The host fluid is water, characterized by density  $\rho_l$  and sound speed,  $c_l$ . We assume that water is at rest and that there are no body forces (gravity) acting. The medium within each sphere is gas, characterized by density  $\rho_g$  and sound speed  $c_g$ . Spatially uniform conditions exist within the bubble and the gas content is constant. The gas temperature equals the liquid temperature, i.e.,  $T_g=T_l= 20^\circ\text{C}$  and remains constant throughout all processes that will be described in this text. Given the parameter values of **Table 1**, the Minnaert resonance frequency for the system under study can be found to be around  $10^6$  Hz, from substitution to  $\omega_M$  (equation (1)). This corresponds to a wavelength of, approximately,  $10^{-2}$  m, meaning that the incident wavelength is several orders of magnitude greater than the size of each bubble. Hence, the bubbly layer can be considered as a metamaterial and will be referred to as bubbly meta-screen in the present text. The bubbly meta-screen radial oscillations in response to an incident sound field are determined by numerically solving, via fourth order Runge Kutta method [17] the Rayleigh-Plesset equation:

$$\frac{d^2R}{dt^2} = \frac{-3}{2} \frac{v^2}{R} + \frac{p_{eq}}{\rho_l R} \left( \frac{R_{eq}}{R} \right)^{3\gamma} - \frac{p_{eq}}{\rho_l R} - \frac{p_{inf}}{\rho_l R} - \frac{4\mu_L v}{\rho_l R^2} + \frac{\delta}{Rh} \frac{d(R^2 R')}{dt} - \frac{2\pi c_l R^2 R'}{Rh^2} \quad (2)$$

The first term on the right-hand side of the equation is the resulting acceleration in the case that the gas bubble is submitted to three forces: the force pointing outwards arising from the gas pressure towards the bubble walls and the two forces pointing inwards due to i) the pressure exerted from the surrounding liquid and ii) the driving pressure field at infinity,  $p_{inf}$ . We assume that the driving pressure field does not affect the bubble shape, hence, the gas bubble stays spherical during the application of the external field. The polytropic law (second term on the right-hand side) calculates the pressure exerted by the gas at a given bubble size by comparing it with the pressure at equilibrium. The polytropic constant,  $\gamma$ , adjusts the relationship between bubble volume and gas pressure and it is often replaced by  $k$  in the literature, as it would play the role of spring constant if we considered the analogy of the mass on a spring from classical mechanics. The last three terms of the equation

account for dissipative losses, as  $\mu_L$  is the viscosity of the surrounding fluid, interactions between bubbles and radiation of acoustic energy. Note that  $R'$  is the derivative of radius  $R$  with respect to time. We assume that the viscosity is zero and as mentioned above there is no heat exchange between the gas and water. Therefore, the energy the bubble loses as it oscillates turns into radiation as expressed by the following relation, equivalent to energy conservation theorem,  $p_{\text{tot}} = p_{\text{inc}} + p_{\text{rad}}$ , where  $p_{\text{inc}}$  is the pressure of the incoming pulse,  $p_{\text{rad}}$ , the acoustic pressure radiated into the surrounding medium and  $p_{\text{tot}}$  is the total pressure field. Here, we cross compare results between two different cases for the incoming pressure. Initially, a Gaussian pulse

$$p_{\text{inc}} = Dpe^{-\frac{(t-t_0)^2}{2\sigma^2}} \quad (3),$$

And, next, a complex frequency pulse described by the formula:

$$p_{\text{inc}} = Dpsinc\left(f_b \left(\left(\frac{t-1.5t_1}{m}\right)^m\right)\right) e^{i2\pi(8f_c)t} H\left(\frac{t}{T}\right) \quad (4),$$

where  $H$ , is the Heaviside step function defined as

$$H\left(\frac{t}{T}\right) := \begin{cases} 1, & \frac{t}{T} > 0 \\ 0, & \frac{t}{T} < 0 \end{cases} \quad (5)$$

impinge upon the bubbly meta-screen, as shown in **Figure 1(a)**. Signals oscillating at complex frequencies, visualized as temporally decaying signals, have been used to induce exotic scattering responses on a dielectric sphere [18], to compensate material loss in plasmonic systems [19], and enhance resolution in an acoustic holey metamaterial [20]. The frequency content of both pulses, determined by the Fourier transformations, is concentrated within a limited range around  $\omega_M$ , as shown in **Figures 1(b)** and **1(c)**. All parameters are given in **Table I**. It is worth noticing that the amount of the input energy carried by the complex frequency pulse is almost half compared to the Gaussian pulse. Moreover, the Fourier amplitude of the latter is six orders of magnitude smaller than that of the complex frequency pulse and the Fourier transformation peak occurs at frequency close to zero, as shown on the top of **Figure 1(b)**. The extremely large Fourier amplitude of the incident complex frequency pulse occurring at frequency close to  $\omega_M$  (shown on the bottom of **Figure 1(b)**) might be associated with persistent interactions demonstrated in the next section. This hypothesis could be tested by solving the Rayleigh-Plesset equation for different complex frequency input pulses, produced either by setting the input pulse parameters close to those of **Table 1** or by using different incident pulse functions. However, the computational experiment should be repeated as many times required by the statistics for the analysis to be valid.

**Table I. Modelling parameters**

Geometrical

Parameters

(m)	Material parameters	Constants	Input pulse parameters
$R_{eq}$ $10^{-5}$	$\rho_l$ $10^3$ kg/m <sup>3</sup>	$\gamma$ 1.4	$Dp=1 \cdot p_{eq}$ , $Dp=2 \cdot p_{eq}$
$h$ $50 R_{eq}$	$c_l$ 1500 m/s	$\delta$ 3.9	$T=\omega_M/c_l = 6.85 \cdot 10^{-6}$ sec
	$\rho_g$ 1204 kg/m <sup>3</sup>		$t_0=1.4$ T
	$c_g$ 343 m/s		$t_1 = 1$ T
	$p_{eq}$ 22798 kg/m·s <sup>2</sup>		$\sigma = 0.1581$ T
	$T_l$ 20° C		$f_b = 1.53 \cdot 10^6$ Hz
	$T_g$ 20° C		$f_c = 1.45 \cdot 10^4$ Hz
	$\mu_L$ 0 Pa·sec		$m=5$

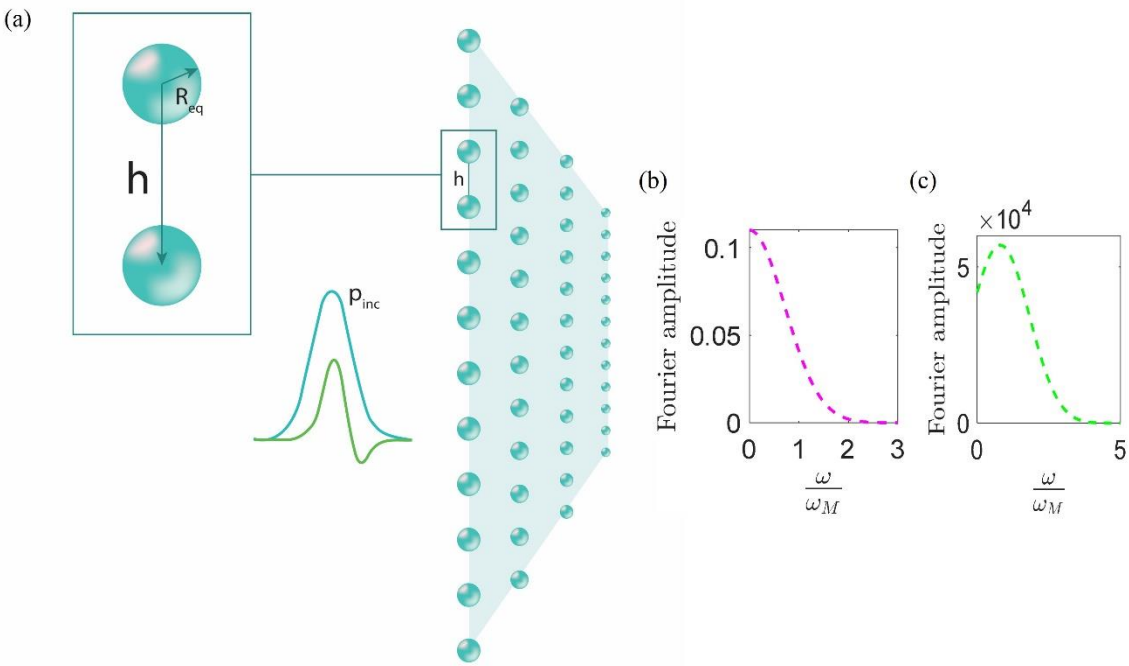


**Figure 1 (a)** Gaussian pulse (petrol solid line) and complex frequency pulse (green solid line) impinging upon the bubbly meta-screen, **(b)** Fourier amplitude versus  $\omega$ , of the Gaussian pulse (magenta dashed line). **(c)** Fourier amplitude versus  $\omega$ , of the complex frequency pulse (light green dashed line).

## Results and discussion

In this section, the radial oscillations of the bubbly meta-screen are presented. The value of the inter-bubble distance  $h$ , as well as the values of the amplitudes of the incident pulses  $D_p$ , have been selected so that the maximum of Fourier transformation of the reflected wave is very close to the Minnaert frequency and the amplitude of the Fourier transformation maximum is relatively small. For incident pulse amplitude values  $D_p = 0.001p_{eq}$  and  $D_p = 4p_{eq}$  (**Figure 2(a)** and **Figure 2(d)**) respectively), the frequency shifts are illustrated as  $h/R_{eq}$  varies. Significant downward shift in frequency and increase in Fourier amplitude maximum can be observed as the inter-bubble distance is decreased from  $h/R_{eq} = 50$  to  $h/R_{eq} = 30$ . These observations are associated with the super-radiation phenomenon, which will not be investigated here as it has been studied elsewhere [21]. Interestingly, for  $D_p = 4p_{eq}$ , two peaks are shown in the reflection spectrum, the upper one moving downwards and the lower one is moving upwards with increasing distance. The upper peak moves towards lower frequencies for increasing  $h$ , because the coupling between bubbles decreases and the array response tends to resemble the single bubble system, in which a single peak is expected in the reflection spectrum. These results could be exploited in sensor applications. We note here that, for time domain ('complex frequency') [22] transient excitation, such as the ones herein, the obtained results are robust against dissipative losses [23], and that our liquid structures are also amenable to a plethora of further (e.g., nonlinear effects [24], [25], potentially allowing for relatively fast modulation [26]).

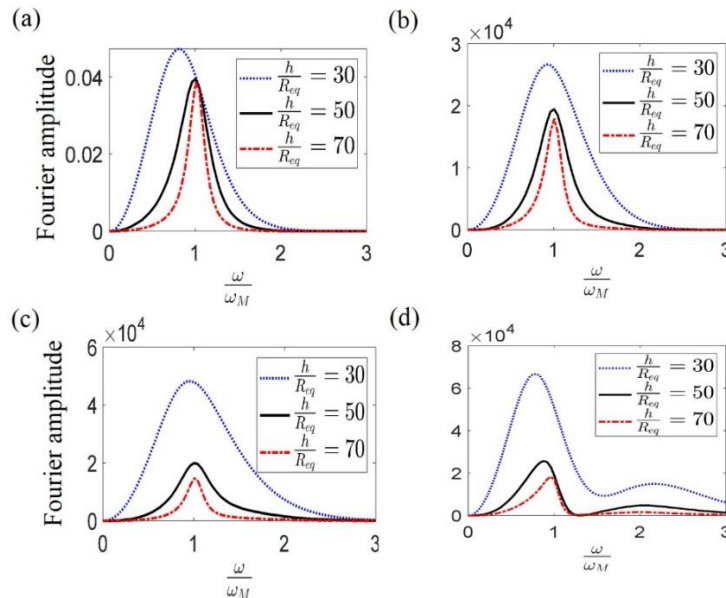


**Figure 2.** Fourier amplitude versus  $\omega/\omega_M$  for different incident pulse amplitude values **(a)**  $D_p = 0.001 p_{eq}$  **(b)**  $D_p = 1 p_{eq}$ , **(c)**  $D_p = 2 p_{eq}$ , **(d)**  $D_p = 4 p_{eq}$ . Results for inter-bubble distance  $h/R_{eq} = 30$ ,  $h/R_{eq} = 50$  and  $h/R_{eq} = 70$  are plotted in blue dashed line, black solid line and red dashed-dotted line respectively.

Except for the long range coupling between the bubbles the frequency shifts are also attributed to the infinite size of the array [27] For incident pulse amplitude values  $Dp=1 p_{eq}$  and  $Dp=2 p_{eq}$  (**Figure 2(b)** and **Figure 2(c)** respectively) the downward shift with increasing frequency is negligible. Additionally, for  $h=50 R_{eq}$  the maximum of the Fourier amplitude of the reflected signal is around  $2 \cdot 10^{-4}$  for  $Dp=1 p_{eq}$  and  $Dp=2 p_{eq}$  (black solid line in **Figure 2(b)** and **Figure 2(c)** respectively), indicating that the amount of the reflected energy for the less dense lattice is smaller. Combinations of those values for the inter-bubble distance and incident pulse amplitudes will be used as inputs to the Rayleigh Plesset equation. Results for the first combination,  $Dp = 1$ ,  $h = 50 R_{eq}$  and for an impinging Gaussian pulse are shown in **Figure 3**. The left vertical axis shows the normalized bubble radius,  $R$ , whereas the vertical axis on the right illustrates the normalized pressure. The pressure of the incident pulse,  $p_{inc}$ , the radiative pressure,  $p_{rad}$  and the total pressure  $p_{tot} = p_{inc} + p_{rad}$  are plotted in pink dotted line, yellow dashed dotted line and black dashed line respectively. At  $t = 2 T$ , the value of the incoming pressure is zero, however, it can be seen that the bubbly-metascreen oscillations persist for up to  $t = 3 T$ , meaning that part of the incident energy is stored in the system. The pulse starts off at  $t = 1 T$ . For  $1 T < t < 1.39 T$ ,  $p_{inc}$  is increasing monotonically while the bubbles' radius are decreasing monotonically as shown in blue solid line; in other words, the bubbles are contracting. For a very short time interval  $1.39 T < t < 1.51 T$ , both  $p_{inc}$  and the bubbles' radius are decreasing monotonically. Next, the *bubbles tend to return to their equilibrium position (i.e. they dilate) during the time interval  $1.51 T < t < 1.76 T$*  and while the pulse's amplitude is decreasing. The first time point (after excitation of the screen) where the pulse's amplitude reaches zero coincides with the time point where  $p_{tot}$  and  $p_{rad}$  cross each other, which is  $t=1.87T$ . From that time point onwards,  $p_{tot}$  equals  $p_{rad}$ . It should be highlighted that the interactions between the incident pulse and the screen are prominent while  $p_{tot}$  is not equal to  $p_{inc}$  since the opposite situation would mean that the presence of the screen has no impact on the

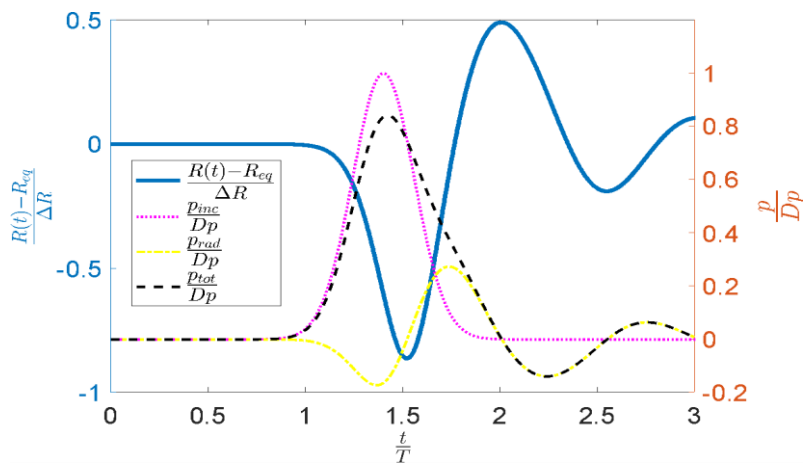


**Figure 3.** Left vertical axis versus horizontal axis: Normalized bubble radius  $R$ , (blue solid lines) versus normalized time  $t$ , for Gaussian excitation with amplitude  $Dp=1 p_{eq}$  and distance  $h=50 R_{eq}$  between neighboring bubbles in a square array. Right vertical axis versus horizontal axis: Normalized i) incoming pressure versus time (pink dotted lines), ii) radiating pressure field versus time (yellow dashed-dotted lines), iii) total pressure field versus time (black dashed lines).  $\Delta R$  is the amplitude of linear undamped oscillations  $\Delta R = \frac{Dp}{3\gamma p_{eq}} R_{eq}$ .

incoming pulse. However, the screen is not transparent and it radiates equal amount of energy in +x and -x directions as soon as the pulse impinges on it. Note that  $p_{tot}$  starts diverging from  $p_{inc}$  at  $t = 1$  T and that the divergence holds for the whole range of times plotted in **Figure 3**, i.e up to  $t = 3$  T.

**Figure 4** shows the oscillations of the bubbly meta-screen for a complex frequency pulse impinging on it. The pulse is illustrated in green solid line and we can distinct three different time intervals. Initially, for  $1.14 T < t < 1.41 T$  the pulse reaches its peak while the bubbles contract. The next time interval,  $1.41 T < t < 1.64 T$ , starts at the time point coinciding with the pulse's peak and terminates at its trough. The bubbles keep contracting in contrast to the previous case where they tended to return to their equilibrium position, thus allowing for energy storage. This statement is enhanced by noticing that  $p_{rad}$  (yellow dotted-dashed line) is decreasing monotonically for  $1.48 T < t < 1.64 T$  and it crosses the  $p = 0$  axis at  $t = 1.68 T$ . At this time point, the bubbly meta-screen fully absorbs the incoming energy, as confirmed by observing the black dashed line crossing the green dotted line; hence,  $p_{tot} = p_{inc}$ . Finally, for  $1.64 T < t < 1.82 T$ , the pulse's amplitude decreases monotonically down to zero while the bubbles' radii fluctuate from the smallest value attained at  $t = 1.64 T$  to an insignificantly larger value and then back to the smallest value. Bubbles at the time point of their maximum contraction instantaneously store the incoming energy and can exert forces on the surrounding fluid or objects placed on it, with potential applications in drug delivery systems. In the present case the bubbles delay to return to their equilibrium position compared to the case the screen was excited by the Gaussian pulse. Specifically they reach equilibrium at  $t = 2.09 T$ , hence 0.33 T later, which corresponds to  $2.26\mu\text{sec}$ . The delay is the result of the complex frequency excitation which drives the system to mainly oscillate in phase with the incoming pulse. It is worth observing that the resulting pressure  $p_{tot}$  (black dashed line) oscillates in phase with the incoming pulse (green dotted

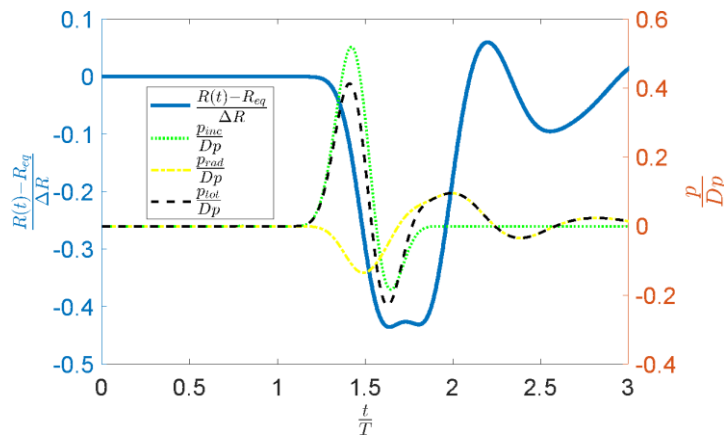


**Figure 4.** Left vertical axis versus horizontal axis: Normalized bubble radius  $R$  (blue solid lines) versus normalized time  $t$ , for complex excitation with amplitude  $Dp=1peq$  and distance  $h=50 Req$  between neighboring bubbles in a square array. Right vertical axis versus horizontal axis: Normalized i) incoming pressure versus time (green dotted lines), ii) radiating pressure field versus time (yellow dashed-dotted lines), iii) total pressure field versus time (black dashed lines).  $\Delta R = \frac{Dp}{3\gamma p_{eq}} R_{eq}$ .

line) and that the bubbles (blue solid line) oscillate in anti-phase with the incident pulse only in the - already described- time interval,  $1.14 T < t < 1.41 T$  and for  $1.17 T < t < 1.18 T$ . Therefore, the total time  $p_{inc}$  and bubbles oscillate in anti-phase is  $0.28T$  whereas for the case of the Gaussian pulse the corresponding time is  $0.64 T$ .

Next, the effect of increasing the excitation amplitude  $D_p$  is examined. The oscillations versus time are shown in **Figure 5** for the case of Gaussian incident pulse ( black dashed line) and complex frequency excitation (red solid line). We have substituted  $D_p=2$  to the formulas defining the incident pulses and the rest of the parameters are fixed to the values shown in **Table I** and are equal to the values which have been investigated so far. The complex frequency pulse triggers  $0.24T$  later than the Gaussian pulse and the pulses terminate simultaneously as shown in **Figure 1**. It can be seen that the first contraction of the bubbles caused by the shortest duration and lowest amplitude , complex pulse is approximately three times larger than that caused by the Gaussian pulse. The impact of the complex frequency pulse on the screen is huge for up to  $t=2.25T$  (second trough illustrated in red solid line) although the value of the amplitude  $D_p$  has only been doubled compared to the previous case studied here. The bubbly meta-screen reaches equilibrium for the first time at  $t=1.17T$  and  $t=2.49T$  for Gaussian and complex frequency excitations respectively. From those time points onwards , the oscillations attenuate , but still, they persist for up to  $t=5T$  as shown in the inset of **Figure 5**, confirming that a complex frequency pulse induces both persistent interactions and intense responses.

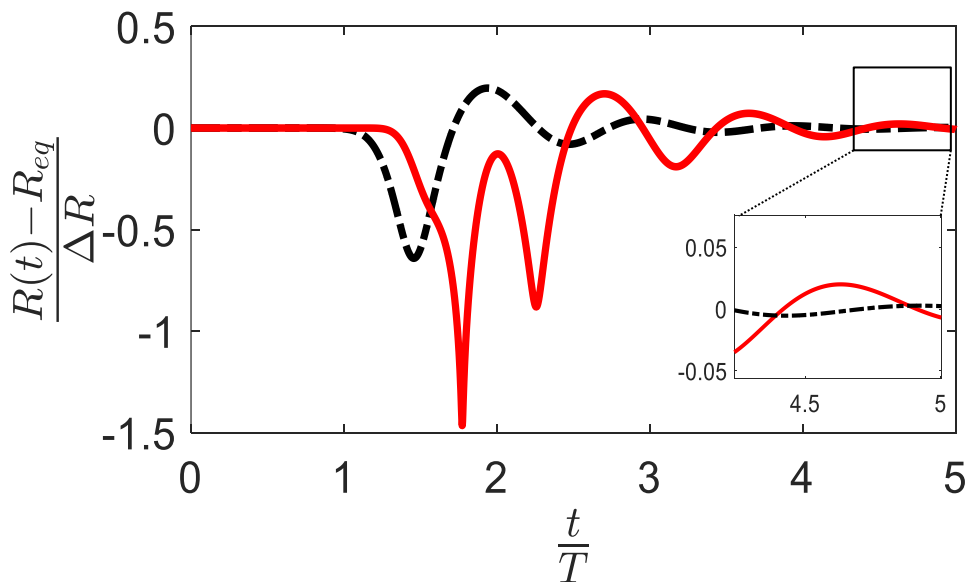


**Figure 5** Normalized bubble radius  $R$  ,(blue solid lines) versus normalized time  $t$ , for a bubble meta-screen with inter-bubble distance  $h=50 R_{eq}$ . Black dashed lines/red solid lines indicate the response in case of an impinging Gaussian pulse/complex frequency pulse respectively. The parameter  $D_p$  has been set to  $2p_{eq}$  in the corresponding equations describing the pulses.

## Conclusion

This work discusses an alternative way to generate oscillations in a bubbly meta-screen, which, to the authors' knowledge has not been reported elsewhere. Triggering a complex frequency pulse with frequency content around the Minnaert frequency tunes the response of the bubbly meta-screen so that the bubbles remain in the contracted state for a couple of moments instead of returning to their equilibrium position. We stress that the amount of energy stored in the bubbly metascreen is increased during those moments and we suggest that further study should be done to optimize the pulse and lengthen the energy storage time. Furthermore, numerical simulations have shown that more intense oscillations as well as persistent interactions can be induced to the screen simply by doubling the amplitude of the incoming complex pulse. These results might be important for future studies where tuning the response of bubble-based metamaterials is desired.

## References

- [1] Strasberg, M. The pulsation frequency of nonspherical gas bubbles in liquids. *The Journal of the Acoustical Society of America*, 25(3), 536-537 (1953).
- [2] Kapodistrias, G., & Dahl, P. H. Effects of interaction between two bubble scatterers. *The Journal of the Acoustical Society of America*, 106(4), 2217-2217 (1999).
- [3] Feuillade, C., Nero, R. W., & Love, R. H. A low-frequency acoustic scattering model for small schools of fish. *The Journal of the Acoustical Society of America*, 99(1), 196-208 (1996).
- [4] Leroy, V., Strybulevych, A., Lanoy, M., Lemoult, F., Tourin, A., & Page, J. H. Superabsorption of acoustic waves with bubble metascreens. *Physical Review B*, 91(2), 020301 (2015).
- [5] V. Leroy, A. Bretagne, M. Lanoy, and A. Tourin, Band gaps in bubble phononic crystals, *AIP Adv.* 6, 121604 (2016).
- [6] Lanoy, M., Lemoult, F., Lerosey, G., Tourin, A., Leroy, V., & Page, J. H., Three-dimensional acoustic lensing with a bubbly diamond metamaterial. *Journal of Applied Physics*, 129 (24) (2021).
- [7] A. Maurel, S. Félix, and J.-F. Mercier, Enhanced transmission through gratings: Structural and geometrical effects, *Phys. Rev. B* 88, 115416 (2013).
- [8] Kafesaki, M., Penciu, R. S., & Economou, E. N., Air bubbles in water: A strongly multiple scattering medium for acoustic waves. *Physical review letters*, 84 (26), 6050 (2000).
- [9] Errico, C., Pierre, J., Pezet, S., Desailly, Y., Lenkei, Z., Couture, O., & Tanter, M., Ultrafast ultrasound localization microscopy for deep super-resolution vascular imaging. *Nature*, 527 (7579), 499-502 (2015).
- [10] Sainidou, R.; Stefanou, N.; Psarobas, I.; Modinos, A. A layer-multiple-scattering method for phononic crystals and heterostructures of such. *Comput. Phys. Commun.* 166, 197–240 (2005).

- [11] Skaropoulos, N. C., Yagridou, H. D., & Chrissoulidis, D. P., Interactive resonant scattering by a cluster of air bubbles in water. *The Journal of the Acoustical Society of America*, 113 (6), 3001-3011 (2003).
- [12] V. Leroy, N. Chastrette, M. Thieury, O. Lombard, and A. Tourin, Acoustics of bubble arrays: Role played by the dipole response of bubbles, *Fluids* 3, 95 (2018).
- [13] Minnaert, M. XVI. On musical air-bubbles and the sounds of running water. *The London, Edinburgh, and Dublin Philosophical Magazine and Journal of Science* 16 (104), 235-248 (1933).
- [14] Horvath, C., Vargas-Hernández, Y., & Cordero, M. L., Minnaert resonance in an array of two-dimensional bubbles. *Physical Review Applied*, 20(4), 044007 (2023).
- [15] H. Ammari, B. Fitzpatrick, D. Gontier, H. Lee, and H. Zhang, Minnaert resonances for acoustic waves in bubbly media, *Ann. I. H. Poincaré - AN* 35, 1975 (2018).
- [16] Pham, K., Mercier, J. F., Fuster, D., Marigo, J. J., & Maurel, A., Scattering of acoustic waves by a nonlinear resonant bubbly screen. *Journal of Fluid Mechanics*, 906, A19 (2021).
- [17] Musa, H., Saidu, I., & Waziri, M. Y., A simplified derivation and analysis of fourth order Runge Kutta method. *International Journal of Computer Applications*, 9(8), 51-55 (2010).
- [18] Kim, S., Lepeshov, S., Krasnok, A., & Alù, A., Beyond Bounds on Light Scattering with Complex Frequency Excitations. *Physical Review Letters*, 129 (20), 203601 (2022).
- [19] F. Guan et al. ,Overcoming losses in superlenses with synthetic waves of complex frequency. *Science* 381,766-771, DOI:10.1126/science.adi1267 (2023).
- [20] Kim, S., Peng, Y. G., Yves, S., & Alù, A., Loss compensation and superresolution in metamaterials with excitations at complex frequencies. *Physical Review X*, 13(4), 041024 (2023).
- [21] Feuillade, C. Scattering from collective modes of air bubbles in water and the physical mechanism of superresonances. *J. Acoust. Soc. Am.* (1995).
- [22] K. L Tsakmakidis et al., *Physical Review Letters* 112, 167401 (2014).
- [23] K. L. Tsakmakidis, A. D. Boardman, O. Hess, Tsakmakidis et al. reply, *Nature* 455, Issue 7216, E11-E12 (2008).
- [24] E. I. Kirby, et al., *Physical Review B* 84, Issue 420, article number 041103 (2011).
- [25] E. Almpanis, et al., *Physical Review B* 101, Issue 51, article number 054412 (2020).
- [26] P. A. Pantazopoulos, et al., *New Journal of Physics* 21 (9), 095001 (2019).
- [27] F. Y. Gardes, et al., *Optics Express* 15, Issue 9, Pages 5879 – 5884 (2007).
- [28] Yoon, S.; Crum, L.; Prosperetti, A.; Lu, N. An investigation of the collective oscillations of a bubble cloud. *J. Acoust. Soc. Am.* 1991, 89, 700–706.